Optimal experimental dynamical decoupling of both longitudinal and transverse relaxations

Xing-Long Zhen,[1] Fei-Hao Zhang,[1] Guanru Feng,[1] Hang Li,[1] and Gui-Lu Long[1,2,3,*]

[1]*State Key Laboratory of Low-Dimensional Quantum Physics and Department of Physics, Tsinghua University, Beijing 100084, P.R. China*

[2]*Innovation Centre of Quantum Matter, Beijing 100084, P.R. China*

[3]*Tsinghua National Laboratory for Information Science and Technology, Tsinghua University, Beijing 100084, P.R. China*

(Received 25 September 2015; published 2 February 2016)

Both longitudinal and transverse relaxations exist in the practical environment. Their simultaneous eliminations are extremely demanding in real applications. Previous experimental work has focused mainly on the suppression of transverse relaxation. In this paper we investigate the performance of three important dynamical decoupling schemes—quadratic dynamical decoupling, periodic dynamical decoupling, and concatenated dynamical decoupling—in an environment with hybrid errors. We propose a method to engineer arbitrary environment by modulating the control field. The technique developed here is universal and can be applied to other quantum information processing systems. Three-dimensional filter functions technique is utilized to analyze the fidelity decay of a one-qubit state protected by dynamical decoupling sequences. This enables us to quantitatively compare the performance of different dynamical decoupling sequences and demonstrate the superiority of quadratic dynamical decoupling in experiments for the first time. Our work reveals that quadratic dynamical decoupling is optimal conditioned on the appropriate noise properties. The difference of constructing dynamical decoupling sequences with various Pauli pulses is also investigated.

DOI: 10.1103/PhysRevA.93.022304

I. INTRODUCTION

Decoherence inevitably exists due to the coupling between a quantum system and baths [1]. The most general one-qubit decoherence Hamiltonian is $H = \sum_{i\in\{0,x,y,z\}} \sigma_i \bigotimes B_i$, where σ_i is the Pauli matrix and B_i is the bath operator. It contains two types of noise: longitudinal relaxation of the population (LR) and transverse relaxation of the phase correlation (TR or dephasing) [2]. To well preserve or precisely manipulate quantum systems, various techniques have been proposed, such as quantum error correction [3], decoherence-free subspace [4–7], dynamical decoupling (DD) [8–10], composite pulses [11], and dynamically error-corrected gates [12,13]. DD, one promising scheme to suppress decoherence, is mainly dedicated to state preservation in quantum memory. Several DD schemes have been proposed, such as the Hahn echo [14], first introduced in the NMR system, CPMG [15,16], periodic dynamical decoupling (PDD) [17], and Uhrig dynamical decoupling (UDD) [18,19]. These schemes exploit the pulse timing and pulse number as free degrees to attain the sequence optimization in the sense of achieving higher decoupling orders with fewer pulses. Among them, UDD has been proved to be able to suppress the pure dephasing of one qubit to $O(T^{N+1})$ in a short duration time T, using only $O(N)$ spin-flip pulses [20–22]. Unlike other DD schemes, UDD contains unevenly spaced pulses, i.e., $T_j = T\sin^2[j\pi/(2N+2)]$, where T_j is the jth pulse timing, and UDD is particularly robust to noise with a hard high-frequency cutoff. The superiority of UDD has been experimentally demonstrated in different systems [23–25].

The system concerned may suffer from errors besides dephasing, induced either by the divulging of the control field or by the redundancy coupling between qubits. Under this condition simultaneous suppression of transverse and longitudinal relaxations requires more complicated DD schemes. One of them is concatenated dynamical decoupling (CDD) [26], in which X and Z (π rotation along the x and z axes in the Bloch sphere) are iterated in the form of $p_{N+1} = p_N X p_N Z p_N X p_N Z$, where p_0 is a time interval τ. Though CDD can achieve the order of the interaction decoupling to $O(T^{N+1})$, the number of pulses needed is around $O(4^N)$, so this scheme is an experimental challenge when N is large. More recently, another scheme, called quadratic dynamical decoupling (QDD), which uses UDD as the building block, has been proposed [27]. In $\mathrm{QDD}_{N_1N_2}$ (the subscript is the decoupling order for TR and LR, respectively), one more layer of the N_1th-order UDD sequence is nested into the interval of the original N_2th-order UDD sequence. So the timing of the pulses $T_{i,j}$ in each interspace of the original UDD sequence is

$$T_{i,j} = T_i + (T_{i+1} - T_i)\sin^2\left(\frac{j\pi}{2N_1+2}\right). \tag{1}$$

The highest order of the population relaxation or dephasing that $\mathrm{QDD}_{N_1N_2}$ can suppress depends on the parity of N_1 and N_2 [28]. But it can be ensured that $\mathrm{QDD}_{N_1N_2}$ can always eliminate the decoherence to $O(T^{\min\{N_1,N_2\}})$ [29]. In a general single-qubit interaction scenario, where $N = N_1 = N_2$, the decoupling order N can be achieved using only $O(N^2)$ pulses [29,30], which is an exponential improvement in the pulse number requirement. Rigorous performance bounds have also been given [31].

Two aspects should be taken into account when considering the sequence performance: the sequence structure and the number of pulses required to eliminate particular noise. The sequence structure features in the designated pulse timing and the form in which pulses are integrated. Once the structure is determined, another degree of freedom we can control is the number of specific pulses. To explain how these two factors influence the operational fidelity, we consider a relative simple scenario, where a one-qubit system is dominated by the dephasing noise. The system Hamiltonian combined with

*gllong@mail.tsinghua.edu.cn

 ©2016 American Physical Society

the control field H_c can be written as $H(t) = H_0(t) + H_c(t)$, where $H_0(t) = S_z \otimes B_z(t) + \boldsymbol{I} \otimes \boldsymbol{B}$. B_z is the component of the bath operator $\boldsymbol{B}$ along the z direction. Let $U_c(t) = \mathcal{T} e^{-i\int d\tau H_c(\tau)}$ signify the control propagator; we can define the toggling frame Hamiltonian $\tilde{H}_0(t) = U_c^\dagger(t) H_0(t) U_c(t)$ and also introduce the notion $\tilde{U}(t)$, which stands for the error propagator satisfying the equation

$$i\frac{d}{dt}\tilde{U}(t) = \tilde{H}_0(t)\tilde{U}(t). \tag{2}$$

The evolution after one DD sequence in the Schrödinger picture can be determined as $U = \mathcal{T} e^{-i\int dt \tilde{H}_0}$. A DD sequence with a superior structure can guarantee the total elimination of the first several Dyson expansion orders of U, even if it contains fewer effective pulses. And under a weak noise regime, lower expansion orders play a decisive role in sequence performance, while in a system where the noise is strong, higher expansion orders will make a difference. Under this condition the pulse number will become a significant factor, and more pulses means greater noise suppression. So we should balance the two essential factors when facing limited resources (see Appendix A).

II. THREE-DIMENSIONAL FILTER FUNCTIONS

Beyond the two aspects we discuss above, another indeterminacy existing in quantum systems is the attribute of the environment. Though experiment feedback can be utilized to accomplish locally optimized DD [32], it will always be beneficial to explicitly predict the sequence efficacy in an arbitrary noisy environment. An important tool for achieving this is the generalized transfer filter function (FF) technique [19,33,34], which offers a novel perspective on understanding the quantum evolution dynamics. Assuming that the system concerned is subjected to classical fluctuation along three axes in the Bloch sphere, we can redefine the respective noise Hamiltonian as

$$H_0(t) = \boldsymbol{\beta}\boldsymbol{\sigma}, \tag{3}$$

where $\boldsymbol{\beta}$ represents the stochastic process along the three principal axes. The toggling-frame error Hamiltonian can be rewritten as [35,36]

$$\begin{aligned}\tilde{H}_0(t) &= U_c^\dagger(t) H_0(t) U_c(t) = \sum_{i=x,y,z} \beta_i U_c^\dagger(t)\sigma_i U_c(t) \\ &= \sum_{i,j=x,y,z} \beta_i R_{ij}(t)\sigma_j = \boldsymbol{\beta}(t)\boldsymbol{R}(t)\boldsymbol{\sigma},\end{aligned} \tag{4}$$

where $\boldsymbol{R}(t)$ is the control matrix, which depends only on the control sequence we apply. For a sequence with consecutive piece-constant control operators $P_l, l \in \{0, \cdots, n\}$, the control matrix at time t in the lth interval has the expression

$$\boldsymbol{R}(t) = \sum_{l=1}^{n} G^l(t)\boldsymbol{R}^{P_l}(t - t_{l-1})\boldsymbol{\Lambda}^{l-1}, \tag{5}$$

where $G^l(t)$ has unit value within the lth time interval and is 0 otherwise. Defining $P_0 = I$, the control matrix for P_l is derived from the Hilbert-Schmidt inner product

$$R_{ij}^{P_l}(t, t_{l-1}) = \tfrac{1}{2}\mathrm{Tr}\big[U_c^\dagger(t, t_{l-1})\sigma_i U_c^\dagger(t, t_{l-1})\sigma_j)\big]. \tag{6}$$

Letting $Q_l = P_l P_{l-1} \ldots P_0$, $\boldsymbol{\Lambda}^{l-1}$ characterizes the cumulative effects of the previous control operators, which has the form $\Lambda_{ij}^{l-1} = \frac{1}{2}\mathrm{Tr}(Q_{l-1}^\dagger \sigma_i Q_{l-1}\sigma_j)$.

The ultimate target is to design one DD scheme such that the actual propagator $U(t)$ is close to identity. We employ the square modulus of the inner product of I and $U(t)$ to evaluate the decoupling performance, i.e.,

$$\mathscr{F} = \tfrac{1}{4}\langle|\mathrm{Tr}(U(t))|^2\rangle. \tag{7}$$

Taking the Magnus expansion of $U(t)$ and working in the weak noise regime, we can neglect the higher orders of the expansion and just keep the first two terms. The fidelity in the time domain is [35,36]

$$\mathscr{F} = 1 - \sum_{i,j,k=x,y,z} \int\int d\tau_1 d\tau_2 \langle\beta_i(\tau_1)\beta_j(\tau_2)\rangle R_{ik}(\tau_1) R_{jk}(\tau_2). \tag{8}$$

We can see that the fidelity decay is determined by the overlap of the noise self-correlation function and the control matrix. Transforming the above equation to the frequency domain, we have

$$\mathscr{F} = 1 - \frac{1}{2\pi}\sum_{i,j,k=x,y,z} \int_{-\infty}^{\infty} \frac{d\omega}{\omega^2} S_{ij}(\omega) R_{jk}(\omega) R_{ik}^*(\omega), \tag{9}$$

where $S_{ij}(\omega)$ is the cross-power spectral density (PSD) between the random variables $\beta_i(t)$ and $\beta_j(t)$ and the control matrix in the frequency domain is

$$\boldsymbol{R}(\omega) = \sum_{l=1}^{n} e^{i\omega t_{l-1}} \boldsymbol{R}^{P_l}(\omega)\boldsymbol{\Lambda}^{l-1}, \tag{10}$$

where

$$\boldsymbol{R}^{P_l}(\omega) = -i\omega \int_0^{t_l - t_{l-1}} dt e^{i\omega t}\boldsymbol{R}^{P_l}(t). \tag{11}$$

For the DD issue, the consecutive operations are simplified as π rotations interleaved with free evolutions. By calculating the respective control matrix, we can use the technique described above to quantify the effectiveness of DD sequences while incorporating the noise influence on pulses. Furthermore, assuming that all the pulses in DD sequences are ideal, i.e., the pulses' power is infinite, we see that Eq. (11) is equal to 0 when P_l denotes π pulses. The interval between pulses is the identity operator so $R^{P_l=I}$ is independent of t and the integral in Eq. (11) can be easily solved. For a DD sequence consisting of n identical X pulses, due to the orthogonality of Pauli operators, the matrix of Λ^{l-1} will only have two nonzero terms, Λ_{yy}^{l-1} and Λ_{zz}^{l-1}, the values of which switch between 1 and -1. When there are pulses executing around different axes in a DD sequence, Λ^{l-1} depends on the specific operations we apply and will always be a diagonal matrix. Similarly, $\boldsymbol{R}^{P_l}(\omega)$ and thus $\boldsymbol{R}(\omega)$ are also diagonal in the bang-bang limit. $|R_{i,i}(\omega)|^2$ represents the noise suppression ability along the i axis in the Bloch sphere. The smaller the product is, the better suppression the DD sequence can achieve. We call $\boldsymbol{F}(\omega) = \boldsymbol{R}(\omega)\boldsymbol{R}^*(\omega)$ the FF matrix and $F_i(\omega) = |R_{i,i}(\omega)|^2$ the FF along the i axis.

Now we can derive the three-dimensional FFs based on Eq. (10) for $\mathrm{QDD}_{3,3}$, CDD_2, and PDD (eight pairs of X and

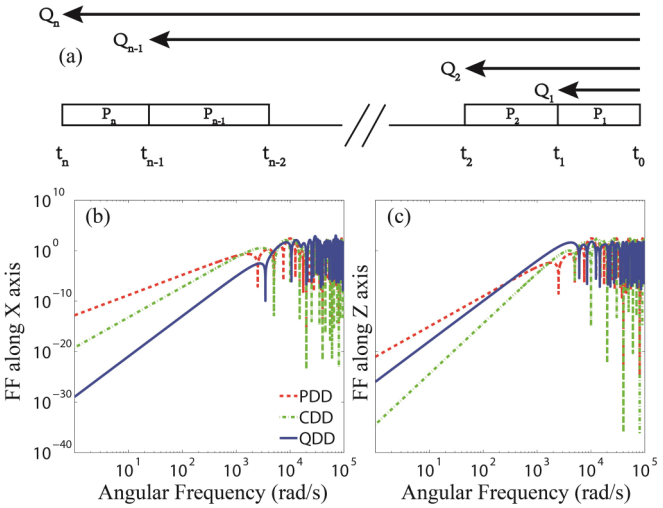

FIG. 1. (a) Schematic of a consecutive piecewise constant control sequence. (b, c) FF values along the x axis (b) and the z axis (c) for $QDD_{3,3}$, CDD_2, and PDD sequences. The total evolution time is fixed at 2.5 ms. The reason we only present the filter functions along the x and z axes is that noise we inject into the system in the experiments along the y axis is absent in the Bloch sphere.

Z evenly spaced pulses). Without loss of generality, Z pulses are nested into X pulses for QDD. Each sequence contains 16 effective pulses and is applied within the same amount of time. Sixteen is the minimum number of effective pulses which not only ensures the equality of pulse resources required but also guarantees the imparity of decoupling order. The results are shown in Fig. 1. We can see that the frequency response is the combined effect of the DD pulse number and the sequence structure. For FF along the x axis, QDD, with the optimal sequence structure and the most Z pulses, has the steepest roll-off, which means that it will have the best performance for eliminating LR noise. However, for TR noise, PDD outperforms QDD after a certain frequency because the pulse number effect outweighs the structure effect. Recent experimental research has focused on one-qubit dephasing issues, in which case only the z component of the FFs is involved. No attempt has been made so far to investigate the practicability of FFs with more than one dimension, even in the DD scenario. Thorough studies on this issue are of great significance since questions may arise with respect to the feasibility of a designed DD sequence in an environment with hybrid errors. Taking QDD, for example, we can gain all the knowledge about whether QDD will be optimal only through its FFs in three dimensions. So we can obtain the actual capability of the protocol to suppress specific noise, lending ourselves to the full evaluation of one DD sequence.

III. EXPERIMENTAL VALIDATION

Three-dimensional FFs can explicitly determine the ability of DD sequences to suppress arbitrary noise. We experimentally verify this in a liquid-state NMR system, where the H nucleus as in the chloroform sample, is the information carrier and the C nucleus is the observing qubit (see Appendix B). One critical obstacle in our experiment is to create a Hamiltonian with hybrid errors since naturally dephasing is the dominating error in our system. The most simple hybrid-error Hamiltonian for one qubit is $H = \beta_z(t)I_z + \beta_x(t)I_x$. The fluctuation of the energy splitting $\beta_z(t)$ can result in TR and the second term $\beta_x(t)I_x$ is responsible for LR. We simulate the Hamiltonian by injecting classic noise into the H qubit. Our method builds on the recent insight that unitary bath engineering can be achieved through modulation of the control field [37,38]. The main idea is to incorporate all the noise terms into the control Hamiltonian and one assumes the presence of a perfectly stable qubit, i.e., there is no ambient decoherence. We first illustrate how to separately engineer LR or TR, and we then present the method of engineering hybrid noise. Following this are our experimental results and discussion.

A. Longitudinal relaxation noise

We inject the longitudinal relaxation noise by rotating the qubit around some certain axis in the X-Y plane with a fluctuating Rabi rate. In this way we simulate the $\beta_x(t)I_x = \hat{\beta}_x(t)\Omega I_x$ term in the Hamiltonian, where Ω is the Rabi rate. $\beta_x(t)$ with the power spectral density $S(\omega) \sim \omega$ takes the form

$$\hat{\beta}_x(t)\Omega = \sum_{j=1}^{N} \alpha_x \sqrt{j\omega_0} \sin(j\omega_0 * t + \phi_j), \tag{12}$$

where $\alpha_{i=\{x,y,z\}}$ is the noise amplitude and ϕ_j is a random phase. $N\omega_0$ determines the high-frequency cutoff, with ω_0 being the base frequency. By changing the form of the coefficient of every term in the summation, we can simulate different types of noise with different PSDs.

B. Transverse relaxation noise

Classical noise that results in dephasing mainly comes from the inhomogeneous and nonstatic magnetic field in our system [1], corresponding to the random variation of the Larmor frequency ω_L. If we neglect the longitudinal relaxation, the initial state $|\psi(0)\rangle = \alpha|0\rangle + \beta|1\rangle$ under the Hamiltonian $\beta_z(t)I_z = \hat{\beta}_z(t)\omega_L I_z$ in the rotating frame after some τ will become

$$\begin{aligned} |\psi(\tau)\rangle &= e^{-i\int_{\tau_1}^{\tau_2}\beta_z(t)I_z dt}(\alpha|0\rangle + \beta|1\rangle) \\ &= \alpha e^{-\frac{i}{2}\int_{\tau_1}^{\tau_2}\hat{\beta}_z(t)\omega_L dt}|0\rangle + \beta e^{\frac{i}{2}\int_{\tau_1}^{\tau_2}\hat{\beta}_z(t)\omega_L dt}|1\rangle \\ &= \alpha e^{-i\Delta\theta_\tau/2}|0\rangle + \beta e^{i\Delta\theta_\tau/2}|1\rangle. \end{aligned} \tag{13}$$

Here $\Delta\theta_\tau$ is the integral of $\hat{\beta}_z(t)\omega_L$. The final state is the same as the one rotated from the initial state by the radio-frequency (RF) pulses for $\Delta\theta_\tau$ along the z axis, i.e.,

$$\begin{aligned} |\psi(\tau)\rangle &= e^{-i\Delta\theta_\tau I_z}(\alpha|0\rangle + \beta|1\rangle) \\ &= \alpha e^{-i\Delta\theta_\tau/2}|0\rangle + \beta e^{i\Delta\theta_\tau/2}|1\rangle. \end{aligned} \tag{14}$$

So if we want to engineer the dephasing noise, we need to rotate the system for $\Delta\theta_\tau$ around the z axis before each decoupling pulse, which imitates the phase change between eigenstate $|0\rangle$ and eigenstate $|1\rangle$ after the previous decoupling pulse due to fluctuation of the magnetic field. Starting with this method, we have to investigate the relationship between the PSD of the

Larmor frequency noise $S_{\beta_z}(\omega)$ and that of the phase change $S_\theta(\omega)$. We obtain that

$$S_{\beta_z}(\omega) \sim \omega^2 S_\theta(\omega). \tag{15}$$

For example, if the $\theta(t)$ we generate before each experiment is

$$\theta(t) = \sum_{j=1}^{N} \frac{\alpha_z}{\sqrt{j\omega_0}} \sin(j\omega_0 * t + \phi_j), \tag{16}$$

the differentiation of $\theta(t)$ gives

$$\hat{\beta}_z(t)\omega_L = \frac{d}{dt}\theta(t) = \sum_{j=1}^{N} \alpha_z \sqrt{j\omega_0} \cos(j\omega_0 * t + \phi_j). \tag{17}$$

The self-correlation function of $\beta_z(t)$ should be [37]

$$\begin{aligned} \langle \beta_z(t)\beta_z(t+\tau)\rangle &= \lim_{T\to\infty} \frac{1}{2T} \int_{-T}^{T} dt \beta_z(t+\tau)\beta_z(t) \\ &= \frac{\omega_L^2 \alpha_z^2}{2} \sum_{j=1}^{N} j\omega_0 \cos(j\omega_0 \tau). \end{aligned} \tag{18}$$

And the PSD is thus the Fourier transform of the self-correlation function:

$$\begin{aligned} S_{\beta_z}(\omega) &= \int_{-\infty}^{\infty} d\tau e^{-i\omega\tau} \langle \beta_z(t+\tau)\beta_z(t)\rangle \\ &= \frac{\pi\omega_L^2\alpha_z^2}{2} \sum_{j=1}^{N} j\omega_0 [\delta(\omega - j\omega_0) + \delta(\omega + j\omega_0)]. \end{aligned} \tag{19}$$

So by generating the phase function, Eq. (17), with the PSD satisfying $S_\theta(\omega) \sim 1/\omega$, we simulate the Larmor frequency noise, with the PSD being $S_{\beta_z}(\omega) \sim \omega$.

C. Hybrid noise

In order to simulate hybrid noise, i.e., LR and TR, one cannot just combine the two methods as we mentioned above since the term $\hat{\beta}_x(t)\Omega I_x$ does not commute to $\hat{\beta}_z(t)\omega_L I_z$. Now we demonstrate how to simulate two kinds of noise simultaneously. In the Schrödinger picture, the Hamiltonian of the qubit and the control field is

$$H(t) = \hat{\beta}_x(t)\Omega\cos(\omega t)\sigma_x + \omega_L[1 + \hat{\beta}_z(t)]I_z. \tag{20}$$

In the rotating frame, under the resonance condition "$\omega \equiv \omega_L$," the Hamiltonian takes the following form:

$$H_r(t) = \hat{\beta}_x(t)\Omega I_x + \hat{\beta}_z(t)\omega_L I_z. \tag{21}$$

In the frame that removes the second term, $\hat{\beta}_z(t)\omega_L I_z$, the Hamiltonian is

$$\begin{aligned} \tilde{H}(t) &= U_z^\dagger(t)\hat{\beta}_x(t)\Omega I_x U_z(t) \\ &= e^{i\int_0^\tau \hat{\beta}_z(\tau)\omega_L I_z d\tau} \hat{\beta}_x(t)\Omega I_x e^{-i\int_0^\tau \hat{\beta}_z(\tau)\omega_L I_z d\tau} \\ &= \hat{\beta}_x(t)\Omega e^{iI_z[\theta_t - \theta_0]} I_x e^{-iI_z[\theta_t-\theta_0]} \\ &= \hat{\beta}_x(t)\Omega[I_x\cos(\Delta\theta_t) - I_y\sin(\Delta\theta_t)]. \end{aligned} \tag{22}$$

Transforming back to the rotating frame, the overall evolution results from the net propagator: $U(t) = e^{-iI_z\Delta\theta_t}\mathcal{T}\exp\{-i\int_{t_0}^{t}\hat{\beta}_x(\tau)\Omega[I_x\cos(\Delta\theta_\tau) - I_y\sin(\Delta\theta_\tau)]d\tau\}$. So in order to create a hybrid noisy environment, $\beta_x(t)$ and $\theta(t)$ are numerically generated with a desired noise power density spectrum and then used to modulate the corresponding RF continuous wave, which will be applied during the interval of the decoupling pulses. The continuous RF waves rotate the qubits at a fluctuating Rabi frequency around a changing axis in the equatorial plane. At the end of the interval an additional rotation around the z axis for the $\Delta\theta_t$ angle is applied. We change the rotating axis by changing the phase of the RF wave and achieve the fluctuating Rabi frequency by modifying the RF-wave output amplitude.

D. Experimental result

As mentioned above, the sequence performance is determined by two essential factors: the sequence structure and specific pulse number. Fixing the total number of pulses, one has to balance the two factors for a given noise environment. In our experiments $QDD_{3,3}$, CDD_2, and PDD are utilized to protect the one-qubit coherence. The sequence duration does not include the π pulse lengths, which is 10 μs each for H nuclei. Also, all pulses are exempt from noise injection and the noise wave between pulses is continuous. Then it can be seen that the self-correlation of $\beta(t)$ is 0 during each pulse and no overlap should exist between $\langle\beta_i(\tau_1)\beta_j(\tau_2)\rangle$ and $R^{P_l=\pi}(t)$ in Eq. (8). So the specific form of pulses is irrelevant to the final fidelity. Therefore the calculations of FF matrices in Sec. II are still valid and can be matched to the experiments we have undertaken. Since the system is clean along the y axis, the operational fidelity can be written as

$$\begin{aligned} \mathcal{F} =& 1 - \frac{1}{2\pi}\int_{-\infty}^{\infty} \frac{d\omega}{\omega^2} S_{xx}(\omega)R_{xx}(\omega)R_{xx}^*(\omega) \\ & - \frac{1}{2\pi}\int_{-\infty}^{\infty} \frac{d\omega}{\omega^2} S_{zz}(\omega)R_{zz}(\omega)R_{zz}^*(\omega). \end{aligned} \tag{23}$$

Neglecting higher order noise cross-correlations and incorporating an approximation to higher order terms, the fidelity has the very simple form

$$\mathcal{F} = \tfrac{1}{2}\{1 + \exp[-\chi(\tau)]\}, \tag{24}$$

where $\chi(\tau) \equiv \frac{1}{\pi}\sum_{i=x,z}\int_{-\infty}^{\infty}\frac{d\omega}{\omega^2}S_{ii}(\omega)R_{ii}(\omega)R_{ii}^*(\omega)$.

The sequence duration cannot be too long since the qubit system is supposed to be stable before any noise is injected. On the other hand, we need discernible experimental results so

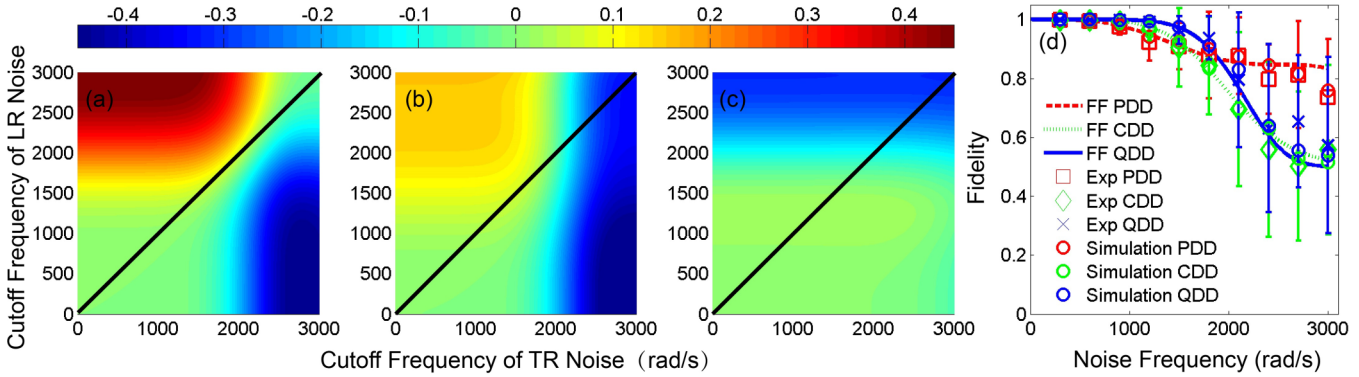

FIG. 2. Fidelity comparison in different kinds of noise environments. The initial state is along the y axis, $\frac{1}{2}(|0\rangle + i|1\rangle)$, and ohmic noise $[S(\omega) \sim \omega]$ is injected into the system. (a–c) Fidelity difference between two arbitrary DD sequences calculated through filter functions (FFs). The duration of all sequences is 2.5 ms. (a) Fidelity difference between $\mathrm{QDD}_{3,3}$ and CDD_2 ($\mathrm{QDD}_{3,3}$ vs CDD_2). The cutoff frequency of dephasing noise is denoted on the horizontal axis; that of LR noise, along the vertical axis. So the region near or in the red zone, with a value above 0, is the region where QDD outperforms CDD. (b) $\mathrm{QDD}_{3,3}$ vs PDD (eight pairs of X and Z evenly spaced pulses). (c) CDD_2 vs PDD. (d) Comparison of the fidelity decay between FF prediction (solid lines) and experimental data (squares, diamonds, and stars) in the partially isotropic noise environment. Each data point is the averaging result of 30 noise realizations. Error bars, two standard deviation units in length each, are presented; the first few are smaller than the data symbols. In all panels $\alpha_x \equiv \alpha_z = 3$ satisfies.

the duration should be long enough to reveal the influence of the noise engineered. Similarly, a noise amplitude that is either too high or too low will not distinguish the efficacy of three sequences. In experiments we choose the duration to be 2.5 ms and $\alpha_{i=x,z}$ to be 3, in general, unless explicitly specified. The explicit results are shown in Fig. 2. The two kinds of noise we injected into the system have the same noise amplitude, i.e., $\alpha_x \equiv \alpha_z$, so the high-cutoff noise frequency ω_{cut} determines which noise dominates the system. When LR is the main noise, QDD has a significant advantage over the other two DD sequences, which can be understood as, since Z pulses are nested into X, QDD has both the highest number of Z pulses and the optimal sequence structure. However, for a pure dephasing noise environment, CDD and PDD will show better protection of the state after a certain frequency, as we can see from the blue zones in Figs. 2(a) and 2(b). This is because when the noise is strong, higher order terms of Dyson expansions of the total evolution propagator $U(t)$ become important. Though $\mathrm{QDD}_{3,3}$ has the strongest suppression for the first several order expansion terms, CDD and PDD can achieve more suppression over the higher orders due to the more effective X pulses. When $\omega^x_{\mathrm{cut}} = \omega^z_{\mathrm{cut}}$, we denote the noise environment as partially isotropic [39], which is indicated by the black line in Figs. 2(a) and 2(b). Experimental data are shown in Fig. 2(d), which shows the consistency of the fidelity decay between FF predictions and experimental data in the isotropic noise environment. Moving to an extreme scenario, where only specific noise exists, we still observe the competition of the pulse number effect and the structure effect as shown in Fig. 3. Numerical simulations are done to estimate the fidelity of experimental data. Noise waves used in the experiments are adopted to derive the ideal final state through Schrödinger equation integration. The absolute distances between the experimental data and the relative simulation results are all below 0.1. Pulse errors are the main sources of experiment infidelities. We eliminate the errors by symmetrizing the pulse phases. But since the single noise injection procedure is equivalent to unitary operations, the symmetry of pulse phases will be damaged when the noise becomes stronger and the pulse errors then cannot be neglected. In the QDD scheme one pulse can be successively applied, which will more easily lead to error accumulation. That is why the experimental data for QDD stray farther from the simulation ones.

So we can conclude that QDD is conditionally optimal and close attention should be paid when it is applied. It is proved that UDD, the building block for QDD, can achieve the best decoupling in baths with an ohmic spectrum and a sharp cutoff, so we inject ohmic noise into the system in order to maximum the capacity of QDD. A weaker performance should be expected if noise with $1/\omega$ spectra is selected. It is also shown that the FF technique is a powerful tool to quantitatively characterize the performance of different DD sequences in all kinds of noisy environments. Of course, the superiority or inferiority of QDD over the other two DD schemes can be

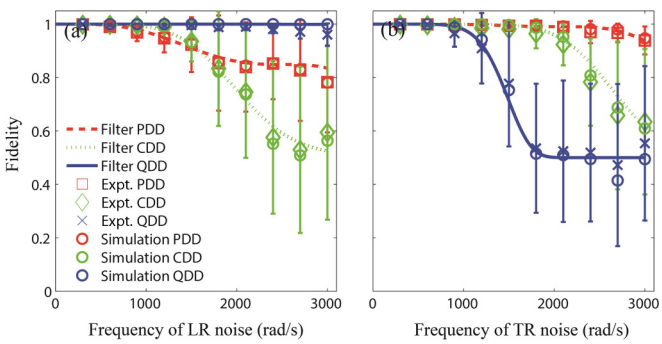

FIG. 3. The performance of QDD, CDD, and PDD in the extreme single LR noise (a) or TR noise (b) environment. Solid lines represent filter-function prediction data; squares, diamonds, and stars, experimental data. Experimental infidelities are also all below 0.1. Each data point is the averaged result of 30 noise realizations. The first few error bars are smaller than the symbols. To magnify the dephasing phenomenon, the noise strength for experiments in (b) is $\alpha_z = 6$ and the sequence duration is 3 ms.

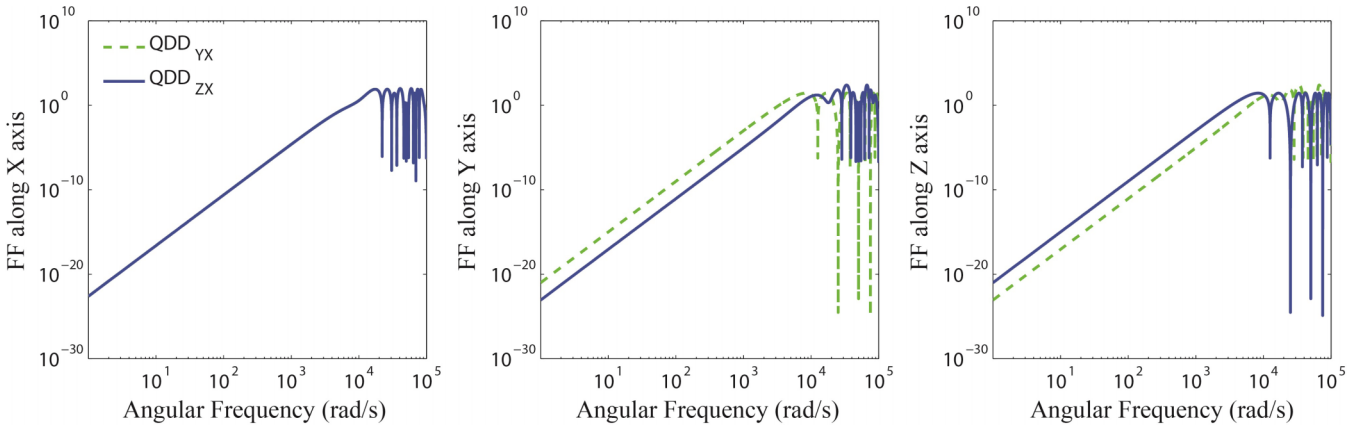

FIG. 4. Three-dimensional filter-function comparison of QDD_{ZX} and QDD_{YX}.

easily seen from the FF analysis. When the noise frequency exceeds the weak region and the convergence assumption is violated, the FF technique becomes less accurate. In this case, the experimental data start to deviate from the fidelity curve predicted by the FF technique as shown in Fig. 3.

IV. SUBSTITUTING Z WITH Y

Alternatively, DD schemes can be constructed with X and Y pulses. Therefore theoretically we consider a one-qubit system with noise Hamiltonian $H(t) = \beta_x(t)I_x + \beta_y(t)I_y + \beta_z(t)I_z$, again assuming that the noise amplitudes along three axes are equal, i.e., $\alpha_x \equiv \alpha_y \equiv \alpha_z$. For $\mathrm{QDD}_{2,2}$ consisting of X and Z as basis pulses (QDD_{zx}), we compare its performance with that consisting of X and Y (QDD_{yx}). Through calculation with Eq. (10), we also derive the three-dimensional FFs for QDD_{zx} and QDD_{yx}. The results show that there is no difference with respect to the state fidelity if the noise environment is really isotropic, in which noise along three axes has the same PSD and high-cutoff frequency. But the noise suppression along the three Bloch-sphere axes differs. If Y (Z) and X pulses are applied, the suppression along the x and z (y) axes will be greater than that along y (z) axis (see Fig. 4). If the noise environment is not isotropic, one has to carefully choose the optimal scheme in order to achieve the best decoupling.

V. CONCLUSIONS

We have studied in detail the experimental elimination of both longitudinal relaxation and dephasing with various DD schemes in the NMR system. The superiority of QDD is experimentally examined and our experiments show that QDD is optimal in most circumstances when the pulse number and sequence structure are considered. An approach to engineering an environment with hybrid noise has been proposed. Three-dimensional FF technique is utilized to study the performance of the various types of DD schemes, and it shows that the performance of a DD scheme depends on both how the pulses are arranged and the number of pulses applied. For a specific noisy environment in a real system, one can first probe the noise spectrum using DD sequences [40] and then construct the optimal decoupling scheme via the FFs. These findings are valuable for practical quantum information processing.

ACKNOWLEDGMENTS

The authors would like to thank Michael J. Biercuk, Greg Quiroz, and Daniel Lidar for useful discussions. This work was supported by the National Basic Research Program of China under Grant No. 2015CB921002 and the National Natural Science Foundation of China under Grants No. 11175094 and No. 91221205. X.L.Z. was supported by Key Laboratory funds (9140C75010215ZK65001).

APPENDIX A: SEQUENCE PERFORMANCE

As mentioned in the text, the evolution after one DD sequence for a one-qubit system dominated by dephasing noise can be determined as

$$\begin{aligned} U^N &= \mathcal{T} e^{-i\int dt \tilde{H}_0} \\ &= I + \sum_{n=1}^{\infty} \int_0^{\tau_{n+1}} d\tau_n \cdots \int_0^{\tau_2} d\tau_1 \tilde{H}_0(\tau_n) \cdots \tilde{H}_0(\tau_1) \\ &= I + \sum_{n=1}^{\infty} \sum_{\vec{\alpha}} \int_0^{\tau_{n+1}} d\tau_n \cdots \int_0^{\tau_2} d\tau_1 \tilde{S}_z^{\alpha_n} \cdots \tilde{S}_z^{\alpha_1} \\ &\otimes B^{\alpha_n} \ldots B^{\alpha_1}, \end{aligned} \tag{A1}$$

where $\vec{\boldsymbol{\alpha}} = \{\alpha_0, \ldots, \alpha_{n-1}\}$. $\alpha_i \in \{0,1\}$ and

$$\tilde{S}_z^{\alpha_i} = \begin{cases} I, & \alpha_i = 0; \\ \tilde{S}_z \equiv U^\dagger S_z U, & \alpha_i = 1; \end{cases}$$

$$B^{\alpha_i} = \begin{cases} \boldsymbol{B}, & \alpha_i = 0; \\ B_z, & \alpha_i = 1. \end{cases}$$

The nth term ($n < N+1$) in the Dyson expansion above consists of 2^n integrals, in which the integrand can be expressed as the direct product of the system and the bath due to the commutation relationship. For each order the system part of the integral is the permutation of the operators $\tilde{S}_z$ and I. When only $\tilde{S}_z$ exists, the integral is 0 under both UDD and PDD. Because of the nature of UDD, the integral with an odd number of $\tilde{S}_z$'s is equal to 0. However, for PDD with the same number of pulses, only the $n = 1$ term can be guaranteed to be fully eliminated,

TABLE I. Comparison of integral values in the first four orders of the Dyson expansion between PDD and UDD. The bath is assumed to be static for the sake of easy calculation. The superscript of $\mathrm{PDD}_N^{(n)}$ (or $\mathrm{UDD}_N^{(n)}$) stands for the expansion order and the subscript denotes the effective pulse number. Numbers in parentheses are the integral values where the integrand consists only of $\tilde{S}_z$, while numbers in brackets are those where the integrand has an odd number of $\tilde{S}_z$'s. We see that integral values with an odd number of $\tilde{S}_z$'s are all 0 for UDD under the condition $n < N$, which is not the case for PDD. But more effective pulses can achieve more suppression for all expansion orders as long as the convergence condition is satisfied.

Sequence	Integrand							
	$\tilde{S}_z$	I						
$\mathrm{PDD}_3^{(1)}$	(0)	1.2337						
$\mathrm{PDD}_7^{(1)}$	(0)	1.2337						
$\mathrm{UDD}_3^{(1)}$	(0)	1.2337						
	$\tilde{S}_z\tilde{S}_z$	$\tilde{S}_z I$	$I\tilde{S}_z$	II				
$\mathrm{PDD}_3^{(2)}$	(0)	[0.003]	[0.003]	0.1903				
$\mathrm{PDD}_7^{(2)}$	(0)	$[7.432 * 10^{-4}]$	$[7.432 * 10^{-4}]$	0.1903				
$\mathrm{UDD}_3^{(2)}$	(0)	[0]	[0]	0.1903				
	$\tilde{S}_z\tilde{S}_z\tilde{S}_z$	$\tilde{S}_z\tilde{S}_z I$	$\tilde{S}_z I\tilde{S}_z$	$\tilde{S}_z II$	$I\tilde{S}_z\tilde{S}_z$	$I\tilde{S}_z I$	$II\tilde{S}_z$	III
$\mathrm{PDD}_3^{(3)}$	(0)	3.2×10^{-6}	1.27×10^{-5}	$[4.584 \times 10^{-4}]$	3.2×10^{-6}	[0]	$[4.584 \times 10^{-4}]$	0.0130
$\mathrm{PDD}_7^{(3)}$	(0)	2×10^{-7}	8×10^{-7}	$[1.146 \times 10^{-4}]$	2×10^{-7}	[0]	$[1.146 \times 10^{-4}]$	0.0130
$\mathrm{UDD}_3^{(3)}$	(0)	7.5×10^{-7}	2.999×10^{-6}	[0]	7.5×10^{-7}	[0]	[0]	0.0130
	$\tilde{S}_z\tilde{S}_z\tilde{S}_z\tilde{S}_z$ $I\tilde{S}_z\tilde{S}_z\tilde{S}_z$	$\tilde{S}_z\tilde{S}_z\tilde{S}_z I$ $I\tilde{S}_z\tilde{S}_z I$	$\tilde{S}_z\tilde{S}_z I\tilde{S}_z$ $I\tilde{S}_z I\tilde{S}_z$	$\tilde{S}_z\tilde{S}_z II$ $I\tilde{S}_z II$	$\tilde{S}_z I\tilde{S}_z\tilde{S}_z$ $II\tilde{S}_z\tilde{S}_z$	$\tilde{S}_z I\tilde{S}_z I$ $II\tilde{S}_z I$	$\tilde{S}_z II\tilde{S}_z$ $III\tilde{S}_z$	$\tilde{S}_z III$ $IIII$
$\mathrm{PDD}_3^{(4)}$	(0)	[0]	$[2 \times 10^{-8}]$	4.9×10^{-7}	$[2 \times 10^{-8}]$	1.2×10^{-7}	1.1×10^{-6}	$[2.949 \times 10^{-5}]$
	[0]	1.2×10^{-7}	1.2×10^{-7}	$[2.8 \times 10^{-7}]$	4.9×10^{-7}	$[2.8 \times 10^{-7}]$	$[2.949 \times 10^{-5}]$	5.027×10^{-4}
$\mathrm{PDD}_7^{(4)}$	(0)	[0]	[0]	3.1×10^{-8}	[0]	8×10^{-9}	6.9×10^{-8}	$[7.733 \times 10^{-6}]$
	[0]	8×10^{-9}	8×10^{-9}	$[4 \times 10^{-9}]$	3.1×10^{-8}	$[4 \times 10^{-9}]$	$[7.733 \times 10^{-6}]$	5.027×10^{-4}
$\mathrm{UDD}_3^{(4)}$	(0)	[0]	[0]	1.16×10^{-7}	[0]	4.62×10^{-7}	0	$[4.91 \times 10^{-7}]$
	[0]	4.62×10^{-7}	4.62×10^{-7}	$[4.442 \times 10^{-6}]$	1.16×10^{-7}	$[4.418 \times 10^{-6}]$	$[4.91 \times 10^{-7}]$	5.027×10^{-4}

yet higher orders of expansions, in which the integral with an odd number of $\tilde{S}_z$'s is not 0, are only suppressed.

In the weak noise regime, lower orders of the expansion determine the total propagator so UDD will outperform PDD even if PDD contains more effective pulses. On the other hand, higher orders will make a difference if the noise is strong and the pulse number will become a significant factor. This character is illustrated in Table I.

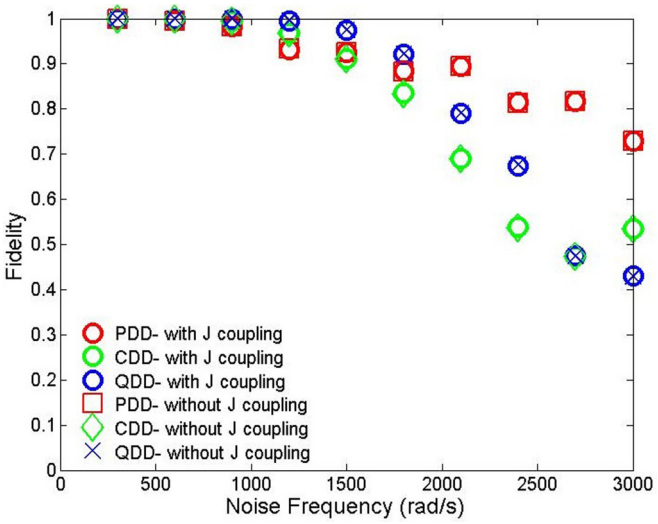

FIG. 5. Fidelity of a single-qubit final state derived from integration of the Schrödinger equation. The initial state is also $\frac{1}{2}(|0\rangle + i|1\rangle)$. The same noise waves are used to modulate H_1 and H_2. Each data point is the average of 30 simulation results. The order of magnitude for the fidelity difference of states driven by H_1 and H_2 is around 10^{-3}, which is far beyond the experimental observation.

Comparing $\mathrm{QDD}_{3,3}$ with PDD with an equal total pulse number and sequence length, for example, we can see that $\mathrm{QDD}_{3,3}$ is superior in the sense that it has the optimal sequence structure and more Z pulses, while it consists of only three effective X pulses, which is far fewer than the eight X pulses that PDD has. So it will be interesting to see if, although consisting of only three X pulses, QDD will always outperform any other sequences in an arbitrary noisy environment.

APPENDIX B: EFFECT OF CARBON NUCLEI

In the chloroform sample, a J coupling interaction exists between hydrogen nuclei and carbon nuclei. The J value is 215 Hz. To show that the coupling barely has any effect on our experiments, we have done two numerical integrations of the Schrödinger equation with different Hamiltonians. One of them contains the J coupling interaction term, denoted $H_1 = 2\pi J 1_z^H 1_z^C + H_c$, and the other one only has the control-field term, $H_2 = H_c$. H_c executes the DD schemes while it implements the noise engineering during the pulse interval. A comparison of the simulation results is shown in Fig. 5, which indicates that the existence of carbon nuclei makes no difference in our experiments.

[1] M. A. Nielson and I. Chuang, *Quantum Computation and Quantum Information* (Cambridge University Press, Cambridge, UK, 2000).
[2] D. Pines and C. P. Slichter, Phys. Rev. **100**, 1014 (1955).
[3] P. W. Shor, Phys. Rev. A **52**, R2493(R) (1995).
[4] P. Zanardi and M. Rasetti, Phys. Lett. A **264**, 94 (1999).
[5] G. Feng, G. Xu, and G. L. Long, Phys. Rev. Lett. **110**, 190501 (2013).
[6] G. Xu and G. Long, Sci. Rep. **4**, 6814 (2014).
[7] S. B. Zheng, Sci. China Phys. Mech. Astron. **55**, 1571 (2012).
[8] L. Viola, E. Knill, and S. Lloyd, Phys. Rev. Lett. **82**, 2417 (1999).
[9] G. F. Xu and G. L. Long, Phys. Rev. A **90**, 022323 (2014).
[10] J. Jing and L. A. Wu, Sci. Bull. **60**, 328 (2015).
[11] J. T. Merrill and K. R. Brown, Quantum Inf. Comput. Chem.: Adv. Chem. Phys. **154**, 241 (2014).
[12] K. Khodjasteh and L. Viola, Phys. Rev. Lett. **102**, 080501 (2009).
[13] K. Khodjasteh, H. Bluhm, and L. Viola, Phys. Rev. A **86**, 042329 (2012).
[14] E. L. Hahn, Phys. Rev. **80**, 580 (1950).
[15] H. Y. Carr and E. M. Purcell, Phys. Rev. **94**, 630 (1954).
[16] S. Meiboom and D. Gill, Rev. Sci. Instrum. **29**, 688 (1958).
[17] L. Viola and S. Lloyd, Phys. Rev. A **58**, 2733 (1998).
[18] G. Uhrig, Phys. Rev. Lett. **98**, 100504 (2007).
[19] G. Uhrig, New J. Phys. **10**, 083024 (2008).
[20] B. Lee, W. M. Witzel, and S. Das Sarma, Phys. Rev. Lett. **100**, 199901(E) (2008).
[21] W. Yang and R. B. Liu, Phys. Rev. Lett. **101**, 180403 (2008).
[22] Y. Pan, Z. R. Xi, and W. Cui, Chin. Sci. Bull. **57**, 2228 (2012).
[23] M. J. Biercuk, H. Uys, A. P. Van Devender, N. Shiga, W. M. Itano, and J. J. Bollinger, Nature **458**, 996 (2009).
[24] M. J. Biercuk, H. Uys, A. P. VanDevender, N. Shiga, W. M. Itano, and J. J. Bollinger, Phys. Rev. A **79**, 062324 (2009).
[25] J. F. Du, X. Rong, N. Zhao, Y. Wang, J. H. Yang, and R. B. Liu, Nature **461**, 1265 (2009).
[26] K. Khodjasteh and D. A. Lidar, Phys. Rev. Lett. **95**, 180501 (2005).
[27] J. R. West, B. H. Fong, and D. A. Lidar, Phys. Rev. Lett. **104**, 130501 (2010).
[28] G. Quiroz and D. A. Lidar, Phys. Rev. A **84**, 042328 (2011).
[29] W. J. Kuo and D. A. Lidar, Phys. Rev. A **84**, 042329 (2011).
[30] L. Jiang and A. Imambekov, Phys. Rev. A **84**, 060302(R) (2011).
[31] Y. H. Xia, G. S. Uhrig, and D. A. Lidar, Phys. Rev. A **84**, 062332 (2011).
[32] H. Uys, M. J. Biercuk, and J. J. Bollinger, Phys. Rev. Lett. **103**, 040501 (2009).
[33] W. B. Dong, R. B. Wu, X. H. Yuan, C. W. Li, and T. J. Tarn, Sci. Bull. **60**, 1493 (2015).
[34] L. Cywinski, R. M. Lutchyn, C. P. Nave, and S. Das Sarma, Phys. Rev. B **77**, 174509 (2008).
[35] T. Green, H. Uys, and M. J. Biercuk, Phys. Rev. Lett. **109**, 020501 (2012).
[36] T. Green, J. Sastrawan, H. Uys, and M. J. Biercuk, New J. Phys. **15**, 095004 (2013).
[37] A. Soare, H. Ball, D. Hayes, X. Zhen, M. C. Jarratt, J. Sastrawan, H. Uys, and M. J. Biercuk, Phys. Rev. A **89**, 042329 (2014).
[38] A. Soare, H. Ball, D. Hayes, M. C. Jarratt, J. J. McLoughlin, X. Zhen, T. J. Green, and M. J. Biercuk, Nat. Phys. **10**, 825 (2014).
[39] Because noise along the y axis is absent in our experiment, the environment is partially isotropic.
[40] J. Bylander, S. Gustavsson, F. Yan, F. Yoshihara, K. Harrabi, G. Fitch, D. G. Cory, Y. Nakamura, J.-S. Tsai, and W. D. Oliver, Nat. Phys. **7**, 565 (2011).